LEAP-GWU-2015 Experiment Specifications, Results, and Comparisons

Bruce L. Kutter[1]*, Trevor J. Carey[1], Takuma Hashimoto[5]‡, Mourad Zeghal[2], Tarek Abdoun[2], Panagiota Kokkali[2], Gopal Madabhushi[3], Stuart Haigh[3], Francesca Burali d'Arezzo[3], Srikanth Madabhushi[3], Wen-Yi Hung[4], Chung-Jung Lee[4], Hao-Chien Cheng[4], Susumu Iai[5], Tetsuo Tobita[5], Takayuki Ashino [5], Jianfei Ren[5],Yan-Guo Zhou[6], Yun-Min Chen[6], Zheng-Bo Sun [6], Majid T. Manzari[7]

Abstract:

LEAP (Liquefaction Experiments and Analysis Projects) is an effort to formalize the process and provide data needed for validation of numerical models designed to predict liquefaction phenomena. For LEAP-GWU-2015, one project within LEAP, an experiment was repeated at 6 centrifuge facilities (Cambridge University, Kyoto University, University of California Davis, National Central University, Rensselaer Polytechnic Institute, and Zhejiang University) and the results were shared and archived for the purposes of validation of numerical models. This paper describes the specifications for the LEAP-GWU-2015 experiment and compares the experimental results from the six facilities. The specified experiment was for uniform medium dense sand with a 5 degree slope in a rigid container subject to a ramped, 1 Hz sine wave base motion. The experiment was meant to be relatively simple to enable different facilities to produce comparable experiments. Although it cannot be claimed that identical experiments were precisely replicated on different centrifuges, it is argued that the results are similar enough that each experiment lends veracity to the set of results. A benefit of variability between experiments is that the variety enables a more general validation. Important lessons with regard to specification of future experiments for validation of numerical models are summarized. LEAP-GWU-2015 has demonstrated an approach that is a useful reference for future validation studies.

Keywords: centrifuge modeling, liquefaction, lateral spreading, numerical simulation, validation, earthquake, pore water pressure

[1] Department of Civil and Environmental Engineering, University of California Davis, Davis, CA, USA
[2] Department of Civil and Environmental Engineering, Rensselaer Polytechnic Institute, Troy, NY, USA
[3] Department of Engineering, Cambridge University, U.K.
[4] Department of Civil Engineering, National Central University, Jhongli City, Taoyuan, Taiwan
[5] Disaster Prevention Research Institute, Kyoto University, Kyoto, Japan
[6] Department of Civil Engineering, Zhejiang University, Hangzhou, P. R. China
[7] Department of Civil and Environmental Engineering, George Washington University, Washington, DC, USA
* Corresponding author: E-mail: blkutter@ucdavis.edu
‡ Former Visiting Scholar, Department of Civil and Environmental Engineering, University of California Davis, Davis, CA, USA

1. Introduction

Numerical models are being developed in academia and are being used increasingly in practice for prediction of the occurrence and consequences of liquefaction [1]. While these codes are used with increasing confidence, there is no practical generally accepted process for validation of capabilities of the numerical implementations of these models. The need for validation, especially for liquefaction phenomena was recognized by VELACS more than 20 years ago [2]. VELACS showed that some numerical procedures were promising but none were reliable. VELACS also showed that there was some difficulty in obtaining reliable data for verification because experiments (especially complex experiments) at different facilities produced different results.

Manzari et al. [3] describes a new international validation effort called LEAP (Liquefaction Experiments and Analysis Projects). Recently, Tobita et al. [4] presented results of numerical predictions of centrifuge tests at different centrifuges in Japan from a LEAP exercise in Kyoto. Although the results of LEAP-Kyoto-2013 and -2014, were a step forward, there were some inconsistencies in the results of centrifuge tests at different universities, primarily because each centrifuge has custom earthquake simulation shaker systems, and the experiments were done in unique, but high-performance, model containers (shear-beam type containers) with different size, mass, and friction characteristics.

It was decided to attempt a new validation effort using a simpler model container, with simple rigid boundary conditions, to more conclusively demonstrate that consistent test results can be obtained at different centrifuge facilities. Simple boundary conditions have the added benefit of reducing complexities of numerical modeling of the special boundary conditions associated with complex model containers. Other papers in this special issue (Tobita et al. [5], Carey et al. [6], Kokkali et al. [7], Hung et al. [8], Zhou et al. [9], Madabhushi et al. [10]) describe unique details of experiments at different facilities. This paper presents specifications and compares results from the centrifuge experiments performed at Cambridge (UK), Kyoto (Japan), National Central University (Taiwan), RPI (USA), UC Davis (USA), and Zhejiang University (China).

Significant effort has been expended to develop procedures to publish the specifications for centrifuge experiments (Carey et al. [11]), to publish and archive experimental data from element tests (Carey et al. [12]), and to publish and archive data from experiments performed at different facilities (Carey et al. [13]). In addition to making direct progress toward validation, an important goal of LEAP-GWU-2015 was to demonstrate a viable approach for validation efforts.

2. LEAP-GWU-2015 Specifications

2.1 Soil material and density

Ottawa F-65 sand was chosen as the standard sand for LEAP-GWU-2015. Ottawa F-65 sand is a clean (less than 0.5% fines), sub-rounded to sub-angular whole grain silica sand, provided by US Silica, in Ottawa, Illinois. Specific gravity and grain size parameters are summarized in Table 1; results from maximum and minimum dry density tests are given in

Table 2; and, an SEM image is shown in Figure 1. Additional material properties of Ottawa F-65 sand, including triaxial, simple shear, and permeability test data, may be found in one of the LEAP databases [12].

Table 1: Specific gravity and grain size characteristics of Ottawa F-65 sand.

	Num of Tests	Average	Stand. Dev.
G_s	4	2.665	0.012
D_{10} (mm)	5	0.133	0.005
D_{30} (mm)	5	0.173	0.009
D_{50} (mm)	5	0.203	0.013
D_{60} (mm)	5	0.215	0.016
Fines (%)	5	0.154	0.133

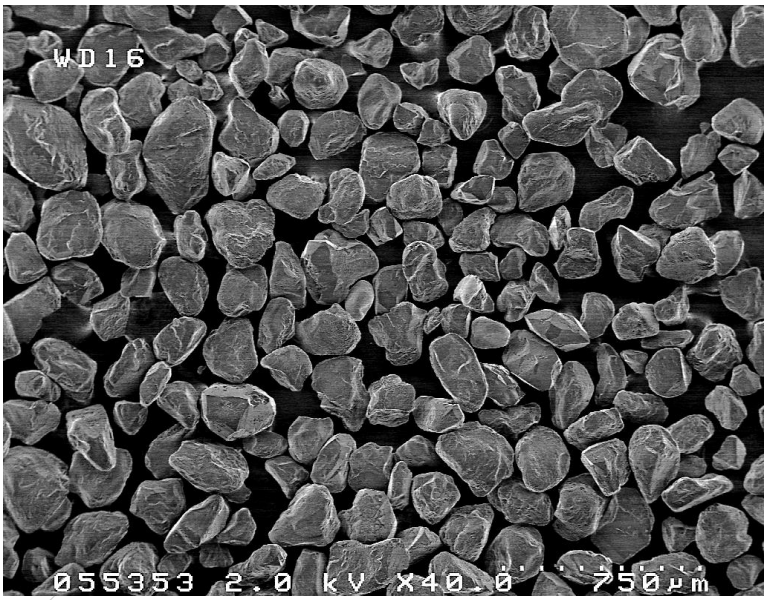

Figure 1: SEM image of Ottawa F-65 sand

The sand in the centrifuge tests was prescribed to be placed at a target density of 1652 kg/m^3. To avoid the small conversion error associated with uncertainty in specific gravity, density was specified instead of the void ratio. From Table 2, it can be seen that considerable scatter is observed in the values of maximum and minimum density. The two experiments performed by professional laboratories according to ASTM D-4253 and 4254, were quite consistent. Assuming that the maximum and minimum dry densities are 1736 and 1515 kg/m^3 respectively, the specified density (1652 kg/m^3) corresponds to a relative density of 65% according to Equation 1.

$$D_r = \frac{\rho_{dmax}(\rho_d - \rho_{dmin})}{\rho_d(\rho_{dmax} - \rho_{dmin})} \times 100 \qquad \text{(eq. 1)}$$

Assuming the maximum values (1538 and 1793 kg/m^3) for index densities would produce a calculated Dr = 48%; and, assuming the minimum values (1406 and 1720 kg/m^3) for index densities would produce a calculated Dr = 82%. Thus it is clear that the values or relative density do involve uncertainty that should be resolved if it is to be the primary index describing the density of sand. It should also be noted that in the centrifuge tests, there are additional systematic and random errors in density from experiment to experiment.

Table 2. Maximum and minimum dry density for Ottawa F-65 sand.

Data source	Test Method	Min. Density (kg/m^3)	Max. Density (kg/m^3)
Cooper Labs (UCD)	ASTM D4254 & D4253	1515	1736
GeoTesting Express (RPI)	ASTM D4254 & D4253	1494	1758
Andrew Vasco (GWU)	ASTM D4254 & D4253	1538	1793
Andrew Vasco (GWU)	Lade et al. [16] (using graduated cylinder)	1521	1774
Cerna Alvarez [14]	Lade et al. [16] (using graduated cylinder)	1415	1720
Cerna Alvarez [14]	Modified ASTM D4254(a)	1406	
Parra Bastidas [15]	ASTM D4254, JIS A 1224	1455	1759
Wen-Yi Hung (NCU)	---	1482	1781
Yan-Guo Zhou (ZJU)	DL/T5355-2006[1]	1456	1733
Average of tests		1475	1756
Stand. Dev. of all methods		46	25

[1]Chinese"Code for soil tests for hydropower and water conservancy engineering", 2006.

The model was composed of Ottawa F-65 sand dry pluviated to a target density of 1652 kg/m^3. Preliminary analysis using the empirical procedure of Idriss and Boulanger [17] with relative density of 65% (estimated as described earlier), and assuming $(N_1)_{60} = 46\ D_r^2 = 19.4$ provides a Cyclic Resistance Ratio, CRR = 0.20. As a first approximation, if one assumes $\sigma_{vc}/\sigma'_{vc} = 2$ and $a_{max} = 0.15$ while assuming magnitude scaling factor (MSF) = 1, depth reduction factor (r_d) = 1, and overburden stress correction factor (K_σ)= 1, the cyclic stress ratio applied to the soil would be

$$CSR = 0.65(\sigma_{vc}/\sigma'_{vc})(a_{max}/g) = 0.20$$

Thus, according to this empirical procedure, the Factor of Safety against liquefaction (*CRR/CSR*) would be approximately 1.0 in a 0.15 g shaking event (Motion #2 shaking event described later).

2.2 Model Geometry

The model is composed of uniform sand, instrumented as shown in Figures 2 and 3, to represent a 5-degree prototype slope dipping downward in X direction along the direction of

shaking. One goal of LEAP is to show that similar results can be obtained on different centrifuges. Some centrifuge facilities have hydraulic shakers that produce 1-D horizontal shaking in the plane of spinning, while other facilities perform the shaking parallel to the axis of the centrifuge. The traditional centrifuge modeling laws do not depend on the centrifuge radius nor on the direction of shaking, but the geometric distortion due to the radial g-field does depend on radius and direction of shaking as discussed in more detail by Carey et al. [12]. Because the g-field is radial in a centrifuge a flat surface in the model would represent a hill in the prototype; erroneous settlements will occur in the experiment due to flattening of the "hill" when the soil is liquefied. To account for the anticipated differences in the radii and shaking direction, the specified model surface was to be curved in the plane of rotation as shown in Figures 2 and 3. In cases where the shaking is in the plane of rotation of the centrifuge, the surface should be a log-spiral shape as indicated in Figure 3. In cases where the plane of shaking is perpendicular to the plane of rotation of the centrifuge, the desired curvature is apparent in section A-A of Figure 2.

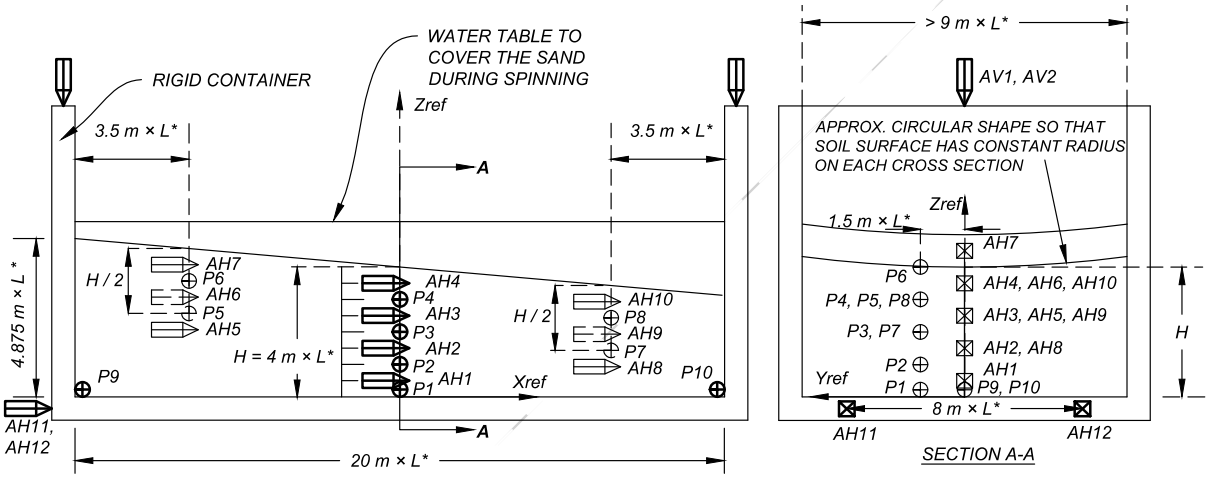

Figure 2: Schematic for GWU 2015 validation experiment for shaking parallel to the axis of the centrifuge.

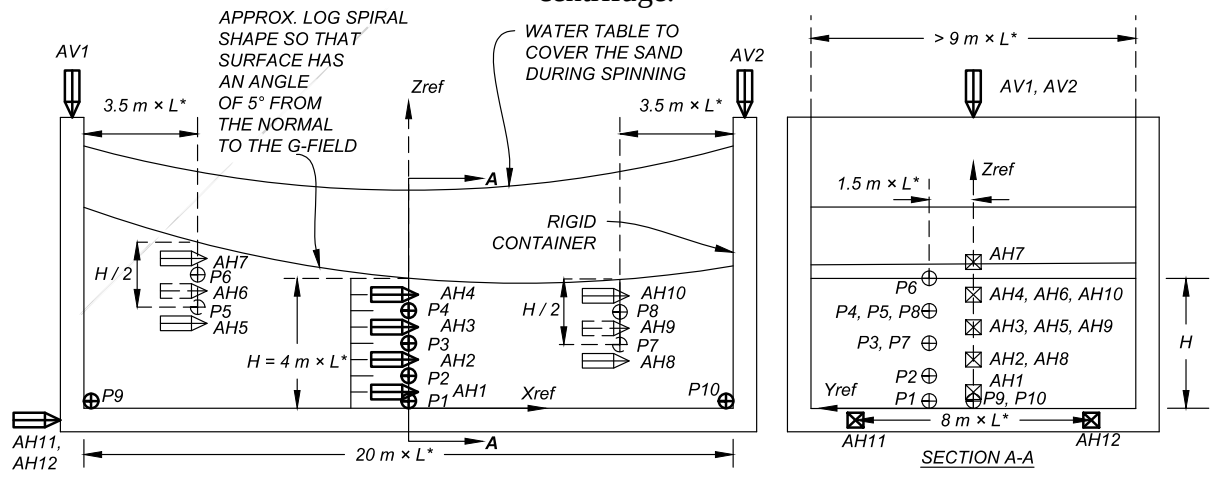

Figure 3: Schematic for GWU 2015 validation experiment for shaking in the plane of spinning of the centrifuge.

In prototype scale, the slope is to be 20 m in length and 4 m deep at the midpoint. The width of the cross section, shown as section A-A in Figures 2 and 3 was specified to be at least 9 m to control boundary effects produced by friction on the sidewalls of the container. The model-scale dimensions and g* are specific to each centrifuge facility, largely determined by the available rigid model containers.

The locations of the accelerometers (denoted by a rectangle and triangle) and pore pressure transducers (denoted by circles) are specified in Figures 2 and 3. Required sensors shown in bold, highly recommended sensors are shown in bold dashed lines, and recommended sensors are shown as non-bolded solid line symbols in Figures 2 and 3.

Required sensors include AH11 and AH12 that measure the achieved base motion and are spaced consistently such that the yaw rotational acceleration can be determined. The vertical accelerometers, AV1 and AV2 are sensitive to container rocking and Coriolis accelerations (which depend on the shaking direction). The central vertical array (P1-P4 and AH1-AH4) were located to minimize their sensitivity to boundary effects from the rigid walls. The pore pressure transducers and accelerometers are offset 1.5 m in the transverse direction (Section A-A) for constructability and reduction of sensor-to-sensor interaction. Centrifuge modelers with access to facilities with large enough containers and data acquisition capabilities were encouraged to include the highly recommended and recommended sensors. The recommend sensors are at equivalent depths as sensors in the central array and are intended to help in understanding the effect of the container boundaries on the model response. Most of the modelers did include some of the recommended sensors. Zeghal et al. [18] – another article in this special issue) performed analysis to evaluate the effects of the side boundaries on the model behavior, and observed that the recordings from the recommended sensors in the arrays near the boundaries are generally consistent with anticipated boundary effects.

2.3 Scaling laws

The scaling laws for centrifuge modeling are described by Garnier et al. [19]. The scale factor for length, L^*, is

$$L^* = L_{model}/L_{protoytype} \quad \text{(eq. 2)}$$

where L_{model} is any length dimension of the centrifuge model and $L_{prototype}$ is the corresponding prototype dimension. The viscosity of pore fluid ($\mu_{model} = \mu_{water}/L^*$) and gravity $g^*=1/L^*$ were to be scaled according to conventional centrifuge scaling laws. The angular velocity, ω, is calculated with the following expression,

$$g^* \times (1g) = g_{model} = \omega^2 \times R_{ref} \quad \text{(eq. 3)}$$

where R_{ref} is the effective radius, taken from the axis of the centrifuge to 1/3 depth of the sand at the location of the central array of sensors. The 1/3 factor minimizes the over and under-stress factors due to varying g-level with radius.

2.4 Surface markers and displacement surveys

Throughout construction and pluviation, the as-placed locations of the accelerometers and pore pressure transducers were to be documented. To determine the extent of surface displacements from liquefaction, a surface marker grid was specified with a maximum spacing of 2 m by 2 m. The markers consisted of cut zip tie heads measuring 10 mm in length and placed in the soil with the top of the head exposed. The entire grid was to be carefully measured before and after saturation, following the first destructive motion, and at the end of the motion sequence.

2.5 Ground motion sequence

The ground motion sequence for the validation experiment was to consist of five motions, three of which could be considered to be non-destructive. All five specified motions of the sequence were a 1 Hz, 16 cycle, ramped sine wave, with the peak of the ramp being the PGA for the specific motion. The first destructive motion (second motion of the sequence) with a PGA of 0.15 g is illustrated in Figure 4. Table 3 summarizes the sequence and intensity of all five motions. The non-destructive motions (e.g. motions 1, 3, and 5) were intended to allow for characterization of the model stiffness after the destructive, main shock motions (e.g. motions 2, and 4). Following Motion #2, the centrifuge was to be stopped and the surface maker grid surveyed.

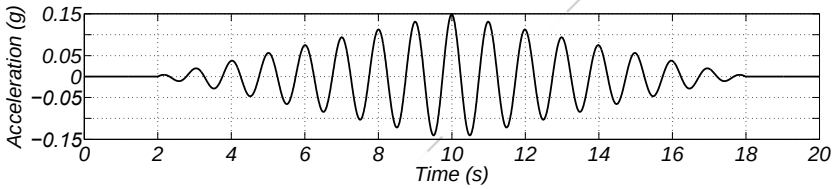

Figure 4: Motion 2 (PGA=0.15g) from the ground motion sequence.

Table 3: Ground motion sequence for GWU 2015 validation experiment

Motion	PGA (g)
1	0.015
2	0.15
Spin down and measure surface makers	
3	0.015
4	0.25
5	0.015

3. Achieved motions and deviations from specifications

This section describes some of the differences between experiments at different facilities and the most significant deviations between specified and as-built models. For more details on construction techniques, saturation process, or other special considerations for each centrifuge

facility refer to the following references (Tobita et al. [5], Carey et al. [6], Kokkali et al. [7], Hung et al. [8], Madabhushi et al. [10], Zhou et al. [9]).

Table 4 summarizes the scale factor, shaking direction, nominal radius of the centrifuge, RPM, pore fluid viscosity and soil density for each experiment. The achieved densities reported by most facilities were very close to the target density of 1652 kg/m^3, though CU reported a significantly lower density, and ZJU reported a larger uncertainty in density. It is believed that the uncertainty in density may have been underestimated at most other facilities. All facilities reported pore fluid viscosities within 15% of the target of $\mu^*/g^* = 1$ except UCD which, due to an error in the calibration of their viscometer, used a pore fluid viscosity 10.9 times greater than specified. Additional details related to the type of viscous pore fluid and details of measurement are documented in the LEAP database (Carey et al. [13]). With the exception of ZJU, which used RC0201 silicone oil, all other centrifuge facilities used a solution of Methylcellulose and water to achieve the required viscosity.

Table 4: Summary of data for each centrifuge facility

Facility	g*	Shaking direction	Nominal radius of centrifuge (m)	Centrifuge radius to 1/3 depth of the model soil (m)	RPM (rev/min)	μ^*/g^*	Density of soil (kg/m^3)
CU	40.0	Tangential	4.125	3.61	99.6	1	1620±20
KU	44.4	Tangential	2.5	2.527	126.4	1.08	1652
UCD	43.0	Tangential	1.0	1.035	193	10.9	1652±10
NCU	26.0	Axial	3.0	2.085	92	0.93	1648
RPI	23.0	Axial	3.0	2.7	87	1.02	1650
ZJU	26.0	Axial	4.5	4.183	74.6	1.15±0.1	1644±54

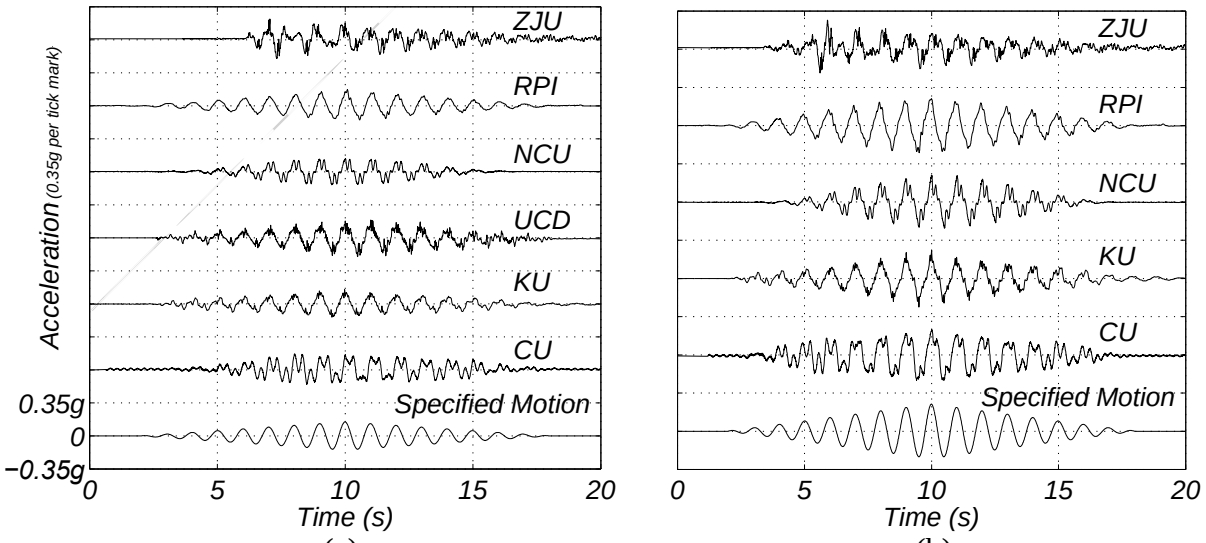

Figure 5: Achieved base accelerations in (a) Motion #2, and (b) Motion #4.

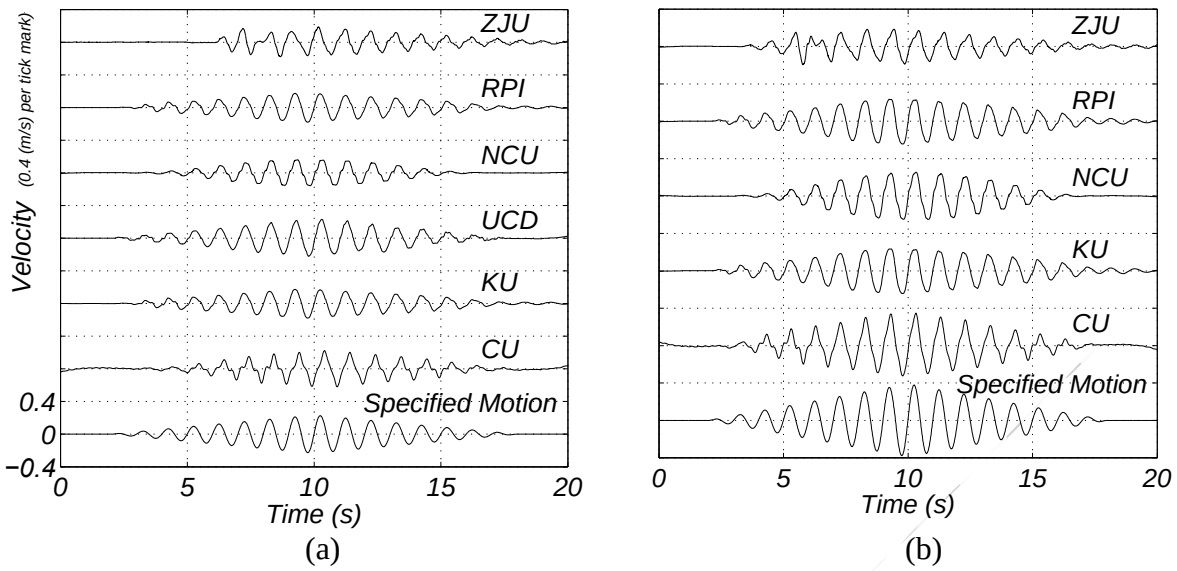

Figure 6: Achieved base velocities in (a) Motion #2, and (b) Motion #4.

The average of the base acceleration measured by AH11 and AH12 is presented as a time series in Figure 5. Figure 6 shows the velocity time series obtained by filtering the base acceleration with a 0.2 Hz high pass filter (for baseline correction) and then integrating with respect to time to obtain velocity. While it is difficult to accurately control high frequency components of the base accelerations using a servo-hydraulic shaker on the end of a spinning centrifuge, the universities participating in this project most did a very good job of producing a smooth base velocity (see Figure 6). The peak base velocity achieved in Motion #4 was only about 60 to 70% of the specified peak velocity for most experiments; the exception was CU which closely matched the specified peak velocity. In Motion #2, the ZJU motions begin rather abruptly and some small cycles are missing prior to the cycle with the peak acceleration. Acceleration response spectra for Motions 2 and 4 are shown in Figure 7. For Motion #2, the achieved peak spectral acceleration at T = 1 s was 0.8±0.2 g at the primary period. For motion #4, with the exception of ZJU, the average peak spectra acceleration at T = 1 s was 1.5±0.2 g. The ZJU and CU motions, and to a lesser extent, UCD, and NCU motions show some higher frequency components in the base acceleration motion.

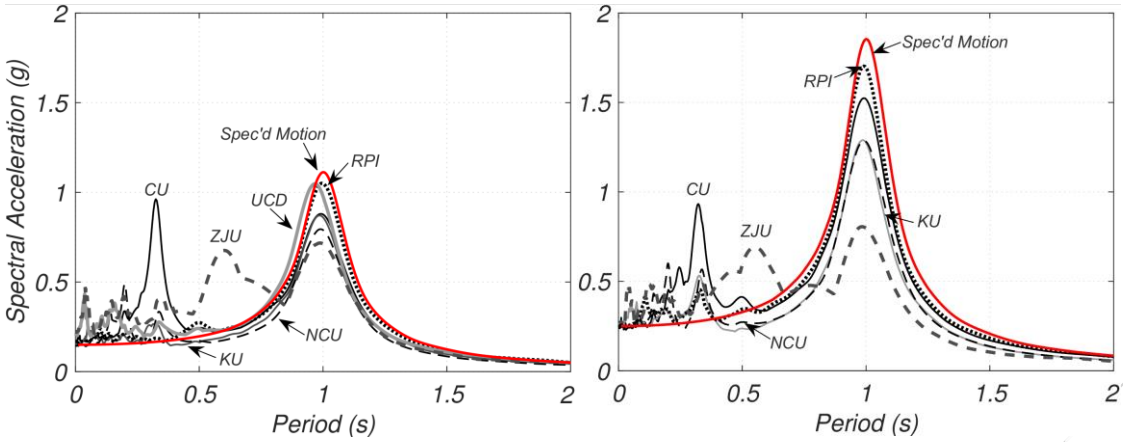

Figure 7: 5% damped acceleration response spectra for (a) Motion #2, and (b) Motion #4.

Separate time series plots from accelerometers AH11 and AH12 are presented as supplementary material for this paper and the electronic results are available for download at (Carey et al. [13]). Except for cases for which one of these accelerometers did not function properly, all of the facilities showed similar accelerations for the two horizontal base accelerometers.

Figure 8 compares the vertical accelerations measured by AV1 and AV2 at opposite ends of the model container for Motion #2. The grey lines indicate the unfiltered motions, and the black lines are band-pass filtered to show the components of the motion between 0.3 and 3 Hz. Although zero vertical acceleration was specified for the experiment, mechanical shaker systems in centrifuges typically produce unintended vertical accelerations in addition to the desired horizontal accelerations. The overturning moment associated with misalignment between the horizontal actuator and the inertial mass of the soil and container causes rocking, which might be exacerbated by resonant frequencies in the vertical or rocking modes. Rocking accelerations are expected to be of opposite sign (180 degrees out of phase) for AV1 and AV2. For the centrifuges with shaking in the tangential direction, Coriolis acceleration will also contribute to the measured vertical acceleration. The Coriolis acceleration, $\bar{a}_{cor} = 2\bar{\omega} \times \bar{v}_{rel}$, depends on the relative velocity of the container in the rotating reference frame and the angular velocity of the centrifuge. For reference, the specified input base velocity for Motion #2 would produce radial (prototype vertical) accelerations of amplitude 0.016 g (prototype scale) for a 2 m diameter centrifuge spinning at 40 g, and this motion would be in phase at the locations of AV1 and AV2. The amplitudes of the vertical components of the filtered motions at the ends of the container range between 8 and 35% of the desired horizontal component. The very high frequency vertical vibrations apparent in the KU motion are not expected to have a significant detrimental effect on the model behavior, though this expectation should be verified.

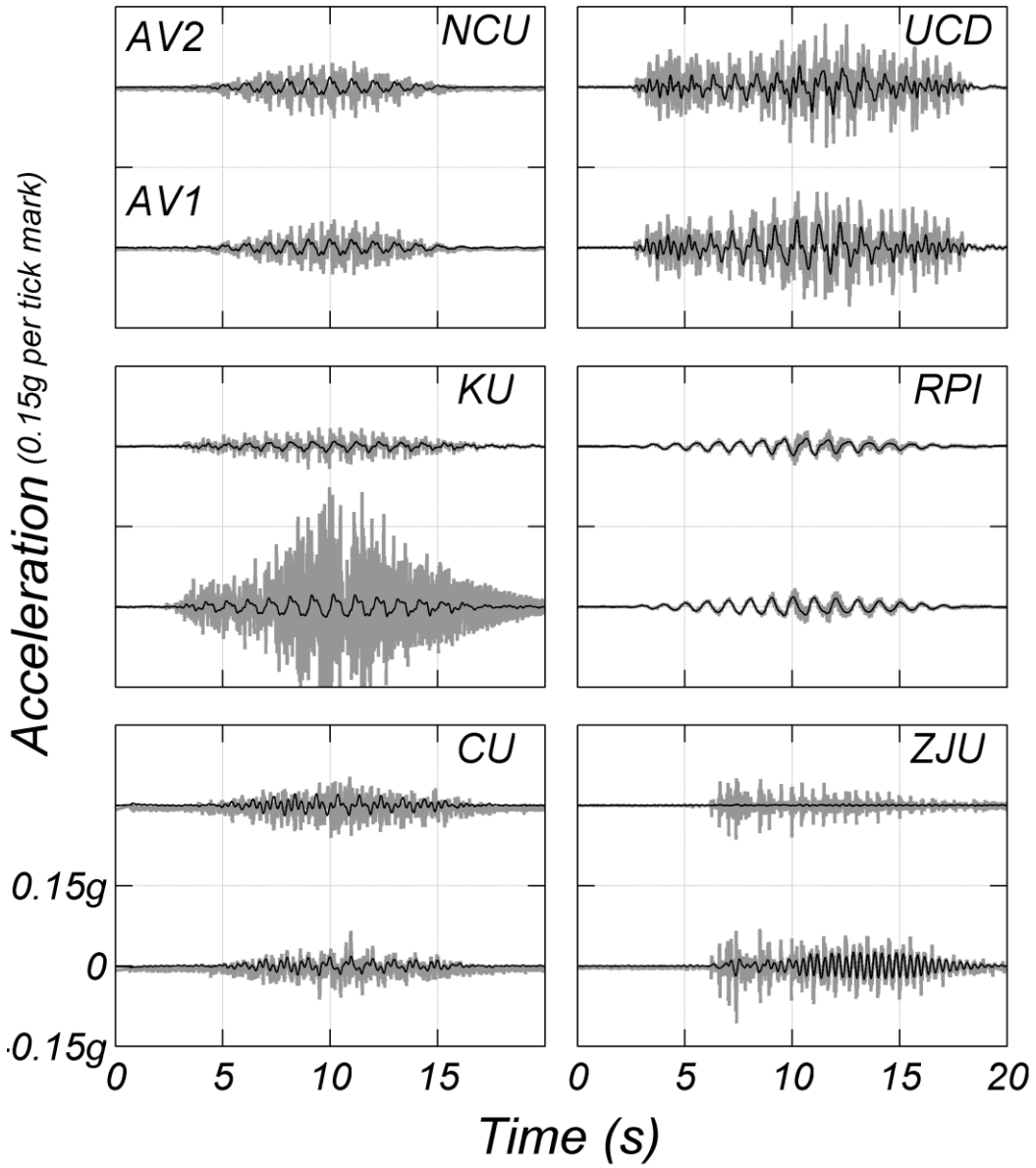

Figure 8: Vertical acceleration measured on container ends. Raw data shown in gray, 0.3 to 3 Hz band pass filtered data is superimposed in black.

4. Results and Discussion

4.1 Pore pressures in the Central Array

Figure 9 shows the response of the central vertical array of pore pressure transducers at all the facilities; (a) shows results for Motion 2 and (b) for Motion #4. P1, P2, P3, and P4 were specified to be at depths of 1, 2, 3, and 4 m respectively, but it should be recognized that the

expected accuracy of sensor locations might be a few tenths of a meter in prototype scale. Overall, the patterns of excess pore pressure generation and dissipation appear to be reasonably consistent for all of the facilities. The pore pressures increase during shaking, and stabilize near the initial effective vertical stress. (For P4, P3, P2, and P1, the initial vertical stresses are approximately 10, 20, 30, and 40 kPa respectively). Excess pore pressures increase with depth. The deeper sensors (e.g. at P1) take longer to build up to their overburden pressure and begin dissipation almost immediately after shaking intensity decreases. The shallow pore pressures (e.g., P4) build up first and stay high longest because pore water drains upward toward the shallow sensors. After excess pore-pressures approach the overburden stress, the large cycles of shaking trigger dilatancy, which produces negative spikes in the excess pore water pressure. In addition to being affected by the extent of liquefaction, the amplitude of these spikes may be sensitive to sensor compliance, and size and permeability of the porous stone. Dilation spikes or de-liquefaction shock waves, described in more detail by Zeghal and Elgamal [20], and Kutter and Wilson [21], are observed at all the centrifuge facilities for both main motions. The cyclic pore pressures at NCU and ZJU have a larger magnitude and are sharper than those measured at the other four centrifuge facilities. Zeghal et al [18] further analyze the pore pressure data and show that the cyclic pore pressures are affected by dilatancy and cyclic lateral stress associated with the rigid boundaries.

4.1.1 Rate of generation of pore pressures

Table 5 summarizes the time to liquefaction at P2 and, the number of cycles to liquefaction at P2 for Motion #2. The time to liquefaction is taken using some judgment from figure 9(a) as the time when the P2 (3 m deep sensor) curve appears to stabilize near 100 % pore pressure. For CU, this sensor did not work, so the time is estimated by interpolating between sensors P1 and P3. The number of 1 Hz cycles to liquefaction is obtained by T_{liq}-2 s, because the earthquake was made of 1 Hz cycles beginning at time = 2 s in Figure 9. NCU, KU, and RPI models liquefied in 10 to 12 cycles. UCD liquefied in 9 cycles, possibly affected by the high viscosity pore fluid used. CU liquefied in only 7 cycles, less than the other tests possibly because their soil was looser, and their input motion contained some high frequency cycles superimposed on the 1 Hz motion. The ZJU model liquefied more quickly, which is reasonable since their motion began rather abruptly, skipping some small cycles prior to the largest shaking pulse, and their base motion did contain significant higher frequency accelerations. The trends in Figure 9(a) and 9(b) are generally consistent with the pattern in the Table 5; KU and RPI pore pressures increase somewhat slower, and Cambridge and ZJU pore pressures increased somewhat faster than pore pressures at UCD and NCU.

Table 5: Pore pressure generation and dissipation rates

Facility	Time to Liquefaction at P2 in Motion 2 (s)	Number of 1 Hz cycles to Liquefaction at P2 in Motion 2	P2, T_{50} for Motion 2	P2, T_{50} for Motion 4
KU	14	12	25	30
RPI	13	11	25	30
NCU	12	10	60	100
CU	9	7	80	120
ZJU	8	6	120	100
UCD	11	9	>>200	---

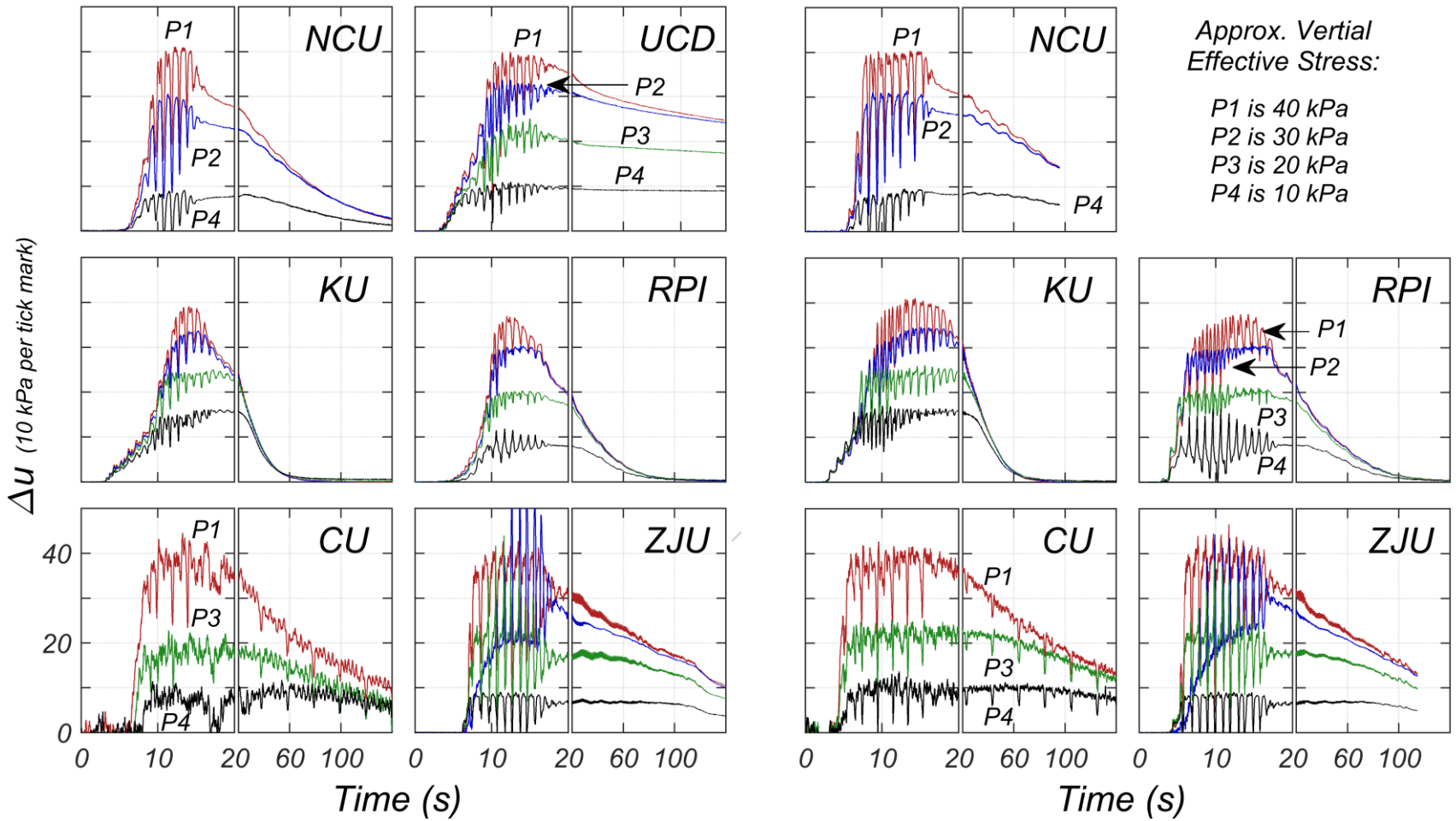

(b) Motion #2 (b) Motion #4

Figure 9: Pore pressure recordings in the central vertical array. The pore pressures are consistently greatest at the bottom (P1) and smallest at the top of the layer (P4) as indicated for Motion #2 (UCD) and Motion #4 (RPI). Other curves are labelled with sensor numbers only if there is a possible ambiguity in the order.

4.1.2 Rate of dissipation of pore pressures

Table 5 compares the time for dissipation of 50% of the maximum pore pressures at P2 in Motions #2 and #4. The pore fluid viscosity of the UCD test was 10.9 times greater than it should have been; as a result, the dissipation times for UCD are much larger than for the other facilities. For the other facilities, the time for dissipation (T_{50}) tended to be greater for models with small number of cycles to liquefaction. For example, in Motion #2 at P2, KU liquefied at t = 14 s, and pore pressures were 50% dissipated in 25 s; CU liquefied sooner (t = 9 s), and pore pressures dissipated later (T_{50} = 80 s). Although this pattern may be explained by a variety of factors, it is consistent with the earlier observation that the sands appeared to be looser than average in the Cambridge and Zhejiang experiments. Looser soils are expected to liquefy earlier and produce more settlement; hence, pore pressure dissipation would be expected take longer for looser soils.

4.1.3 Motion 2 compared to Motion 4

UCD did not perform Motion #4, For ZJU, the Motion #4 was very similar to Motion #2. For the other universities, Motion #4 (0.25 g target) was significantly stronger than Motion #2 (0.15 g target); in Motion #4 liquefied was triggered in fewer cycles and the time required for dissipation increased (T_{50} in Table 5). The pore pressure sensors in the soil produced larger negative spikes of pore pressure and acceleration in Motion #4 as compared to Motion #2.

4.2 Accelerations in the Central Vertical Array

Figure 10 presents the recorded accelerations for Motions 2 and 4. If they showed evidence of significant drift, the accelerations were filtered using a 0.2 Hz high pass filter. The order of the traces in each plot correspond to the depth of the sensors; AH4 was specified to be 0.5 m from the surface of the sand with AH3 – AH1 successively spaced at 1 m depth increments below this in the model. Before liquefaction, the shape of the acceleration traces are very similar to the base motion. After liquefaction, the waveform is very distorted, sometimes hovering near zero with occasional dilation spikes associated with cyclic de-liquefaction and re-liquefaction; these spikes have been observed by many researchers studying centrifuge and field data (e.g., Zeghal and Elgamal [20], Bonilla et al. [22]). The formation of de-liquefaction acceleration and pore pressure spikes is described in the context of shock waves by Kutter and Wilson [21]. The dilatancy spikes are apparent in all six experiments. The spikes tend to be most exaggerated near the ground surface. The spikes are unsymmetrical due to the presence of the sloping ground; the dilatancy spikes are triggered more extensively for strains occurring in the direction of the static shear stress. Looking closely at timing of the spikes, it is possible to deduce a wave velocity for the spikes of approximately 10 to 20 m/s.

The velocity of propagation and the sharpness and amplitude of the spikes is a function of the ground motion, and the extent of liquefaction. The thickness of the accelerometer relative to the length of the shock wave front could also affect the recordings of spatially sharp wave fronts. The prototype size of the accelerometers (sensor thickness in the vertical direction multiplied by the length scale factor, L*, is listed in Table 6.

Table 6. Dimensions of Buried Sensors

Centrifuge Facility	Accelerometer thickness (prototype mm)	accelerometer type and model number	PPT porous stone diameter (prototype mm)	PPT type and model number
CU	380	Piezoelectric, D.J. Birchall Model A-23	254	Druck PDCR-81
KU	266.4	SSK, model A6H-50	244.2	SSK model P306A-2
UCD	300	ICP PCB 352M54	207	Keller 2Mi-100-81840
NCU	200	PCB W353B17	164	Druck PDCR81-3 bar
RPI	164	PCB Piezotronics Model 353B17	161	Keller Model 2MITAA 81840.1
ZJU	416	KYOWA AS-100HA	166	Druck PDCR81

4.3 Pore Pressure Response P9 and P10

The purpose of requiring P9 and P10 was largely for quality control and for assessment of boundary effects. Results for Motion 2 are presented in Figure 11.

Due to the curvature of the soil surface, the depth of soil above P9 and P10 is greater for centrifuges with a tangential shaking; thus greater excess pore pressures are possible and greater excess pore pressures were observed in the KU, UCD, and CU tests. On the other hand, the depth of potentially liquefiable soil above P9 is greater than above P10, yet peak excess pore pressures are smaller at P9 than at P10. The differences in P9 and P10 during shaking seem less significant in Motion 4 (shown in an appendix or on-line supplementary material).

Centrifuges with shakers that shake in the direction of the axis of the centrifuge have platforms that swing in the plane of the shaking. So, if friction was present in the swing bearings and the friction was released by shaking, the bucket would rotate during shaking. Such a rotation, if significant, could be detected by comparing residual pore pressures measured at P9 and P10. Based on analysis of the residual pores pressures at P9 and P10 (not shown) the rotation of the bucket associated with swing bucket friction was not significant.

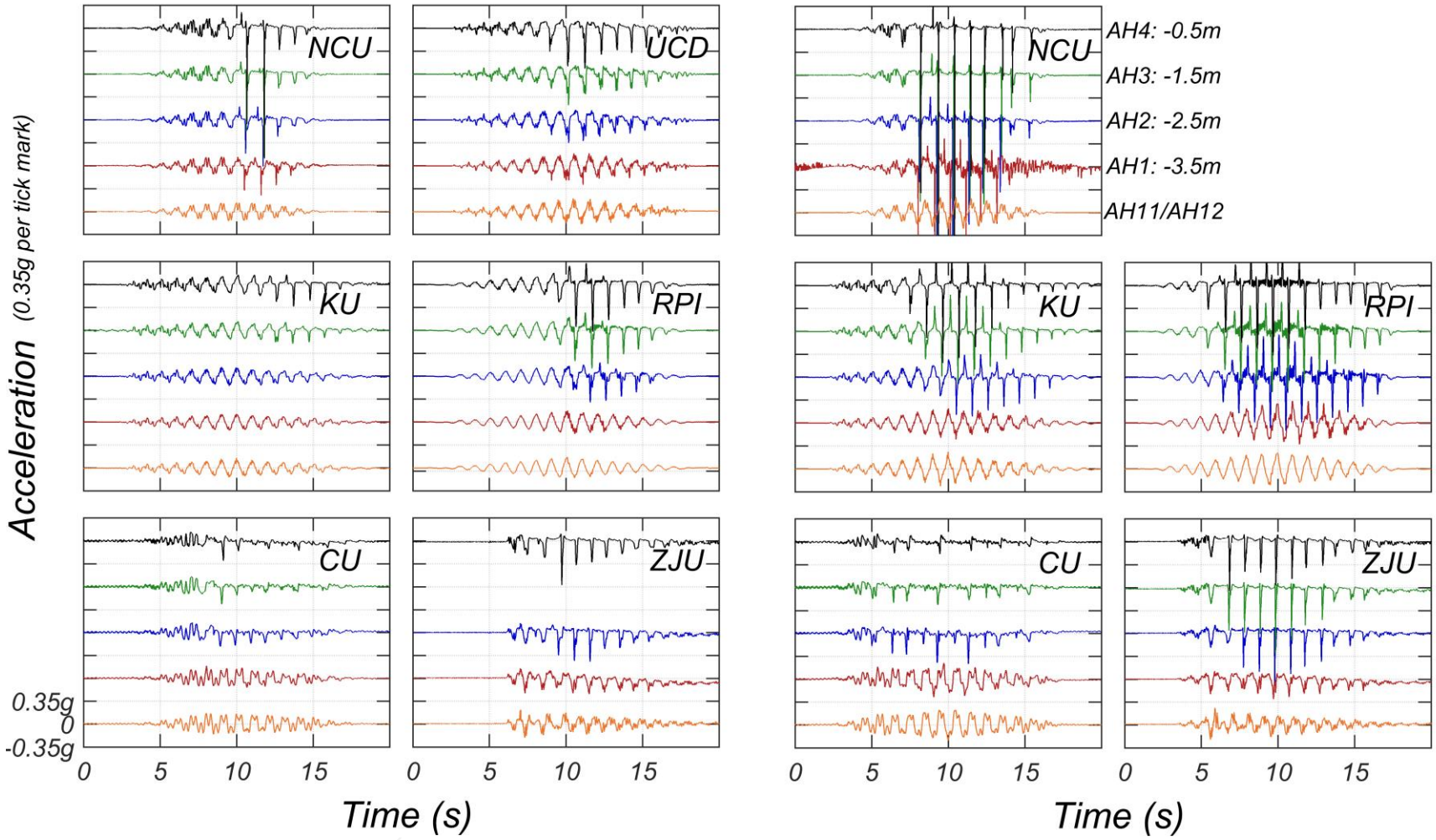

Figure 10: Horizontal accelerations in the central array for Motion #2 (left) and #4 (right). For each subplot the sensors are arranged according to their depth (AH4 at the top and AH1 at the bottom). Specified depths are indicated next to the top right of the figure.

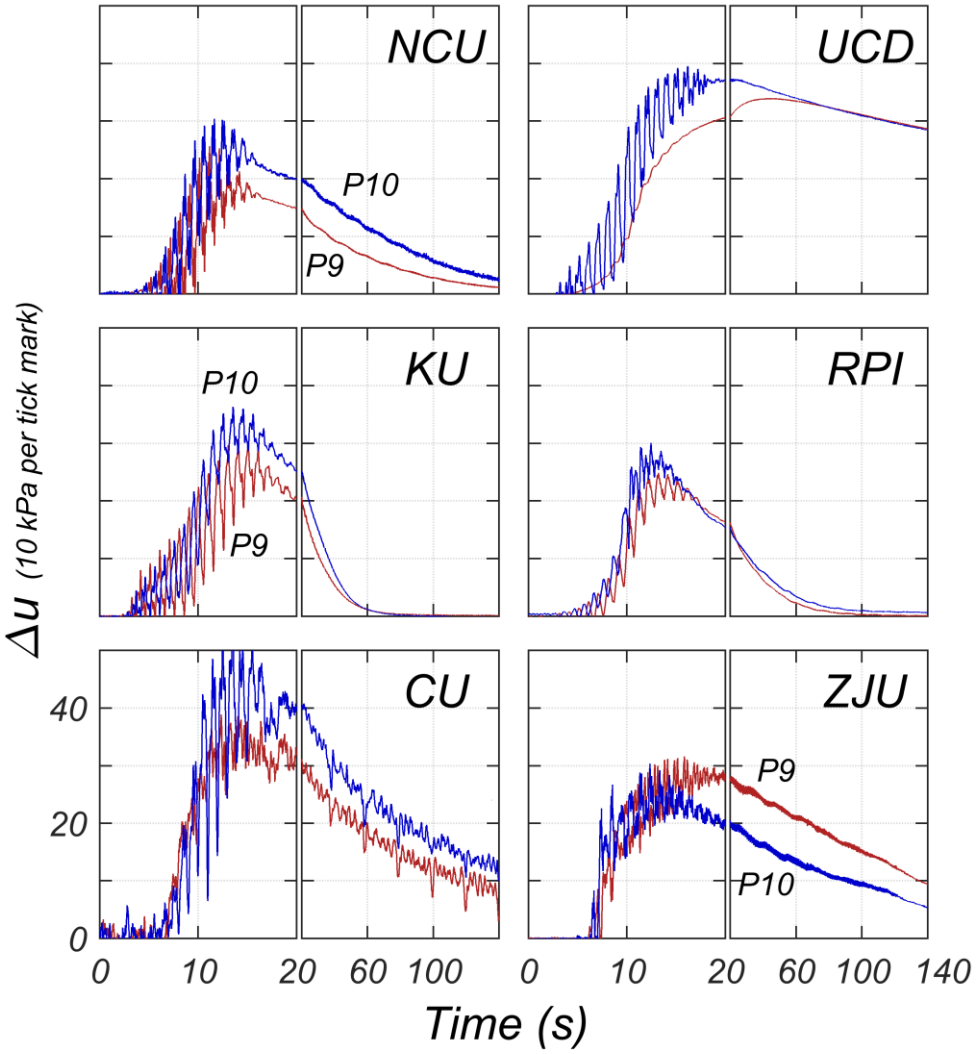

Figure 11: Pore pressure response during Motion #2 for P9 and P10 located on the base of the container.

4.4 Comparison of Central and Side Arrays

The cyclic shear strains are constrained by the side boundaries of the rigid container (especially the end walls), and hence one may expect liquefaction to occur more easily in the middle of the container, far from the end walls. Figure 12 compares results in the central array to results nearer the left and right sides of the container to help in assessing the importance of the walls of the container on the model response. Results are not given for every experiment because sensors P5, P7, AH6, and AH9 were not required to be included in the models. Figure 12 shows pore pressures from sensors P5, P3, and P7 that were specified to be placed at a depth of 2 m at different points along the slope for Motions 2 and 4. There is a trend, which might be significant, that the cyclic pore pressure in the central array (P3) have a somewhat different character than the pore pressures at P7 and P5. In the RPI test, P3 appears to reach greater pressure than P5 and P7, though this could be explained by the fact that P3 was deeper than P5 or P7 (as opposed to boundary effects) in the RPI test.

Figures 12c and 12d shows accelerations from sensors AH6, AH3, and AH9, that were specified to be placed 1.5 m below the ground surface at different points along the slope. It may be significant that the magnitudes of the spikes tend to be greatest in the middle of the container (i.e., at AH3). Large spikes in the acceleration and pore pressure at the middle of the container would be consistent with the expectation that liquefaction is likely to occur first and to be most extensive in the middle of the container.

4.5 Soil Surface Marker Displacement

Figures 13 and 14 present the vertical and lateral surface displacements for Motion #2 and #4. The vertical displacements were measured for the row of surface markers along the longitudinal centerline and the lateral displacements for the markers near the transverse centerline. Motion #2 displacements include incremental deformations that occurred between the end of saturation and stopping the centrifuge after Motion #2. Motion #4 displacements are the incremental displacements after Motion #2.

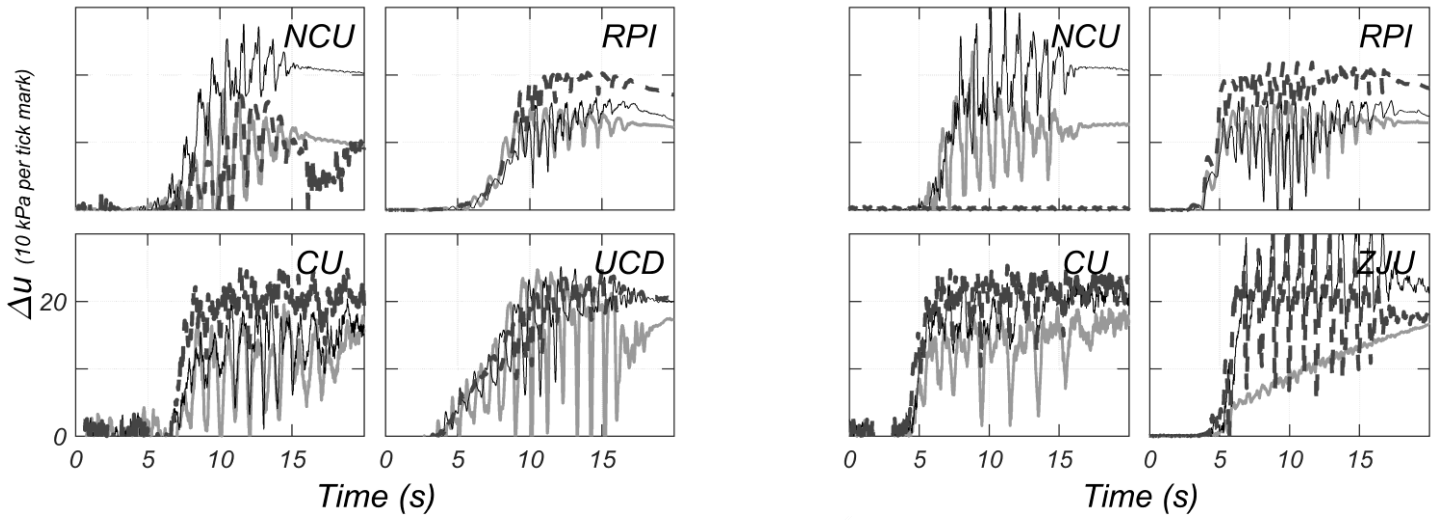

(a) Motion #2 **(b) Motion #4**

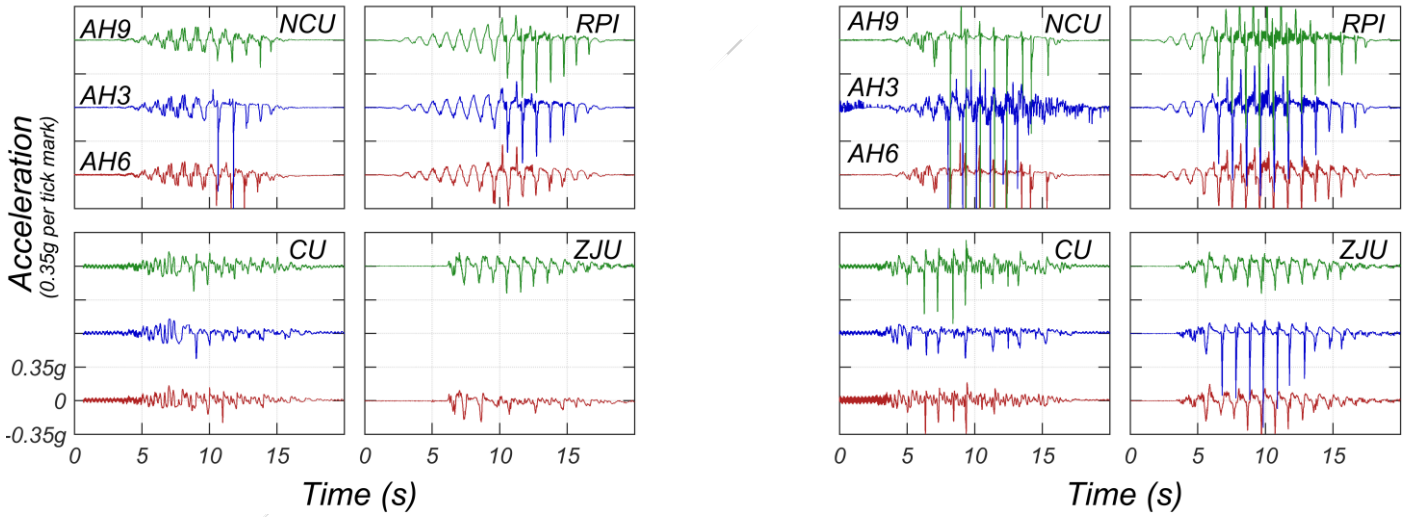

(c) Motion #2 **(d) Motion #4**

Figure 12: Excess pore pressure recording for (a) Motion# 2, (b) Motion #4, and horizontal shaking recording for (c) Motion #2 and (d) Motion #4.

4.5.1 Vertical Displacements

For all experiments, the soil surface settles at the top of the slope for both motions. At the toe, the magnitude of the settlements is much smaller, with some experiments reporting heaving. The surface displacement pattern for Motion #2 (Figure 13b) is consistent among the different experiments. Motion #4 displacements are larger in magnitude and the soil surface displacement pattern is less consistent. Note that the irregularity of the shapes is likely associated with measurement error; the magnitude of settlements was not much greater than the accuracy of the measurements in most cases.

4.5.2 Lateral Displacements

KU, UCD, and RPI all reported similar lateral displacement patterns both in terms of magnitude and shape for Motion #2 (Figure 14). ZJU had the largest lateral displacements with an average reported value of 0.55 m. It was anticipated that lateral displacements would be maximum in the middle of the container (i.e., at Y = 0), similar in shape to the profile for ZJU in Figure 14(c). One interesting observation from Figure 14(b) is that UCD, KU and RPI showed a local minimum of lateral displacement in the center of the box. The limited sample size along with the limited accuracy of the manual measuring tools would produce uncertainties on the order of 0.03 m in the measurements (1 mm model scale corresponds to 0.02 to 0.05 m prototype scale depending on the scale factor adopted). The displacement patterns for Motion 4 are similar for KU and RPI. ZJU measured displacements for Motion #4 that are similar to Motion #2. The lateral displacements patterns are less consistent for Motion #4.

4.6 Horizontal Relative Displacement

Figure 15 shows the computed horizontal relative displacement of the AH4 relative to the base for Motions 2 and 4. The horizontal displacement combines relative dynamic displacement and average permanent displacement from surface markers near the middle of the container reported in Figures 14.

4.6.1 Method of Calculating Horizontal Relative Displacement

The dynamic displacements, shown by gray lines in Figure 15, were obtained by subtracting acceleration at AH4 from the acceleration at the base of the container, and then double integration with respect to time. Following each integration, a 0.2 Hz high pass filter was applied to remove drift. Double integrating acceleration data to determine dynamic displacement is similar to a process presented by Ghaffar and Scott [23].

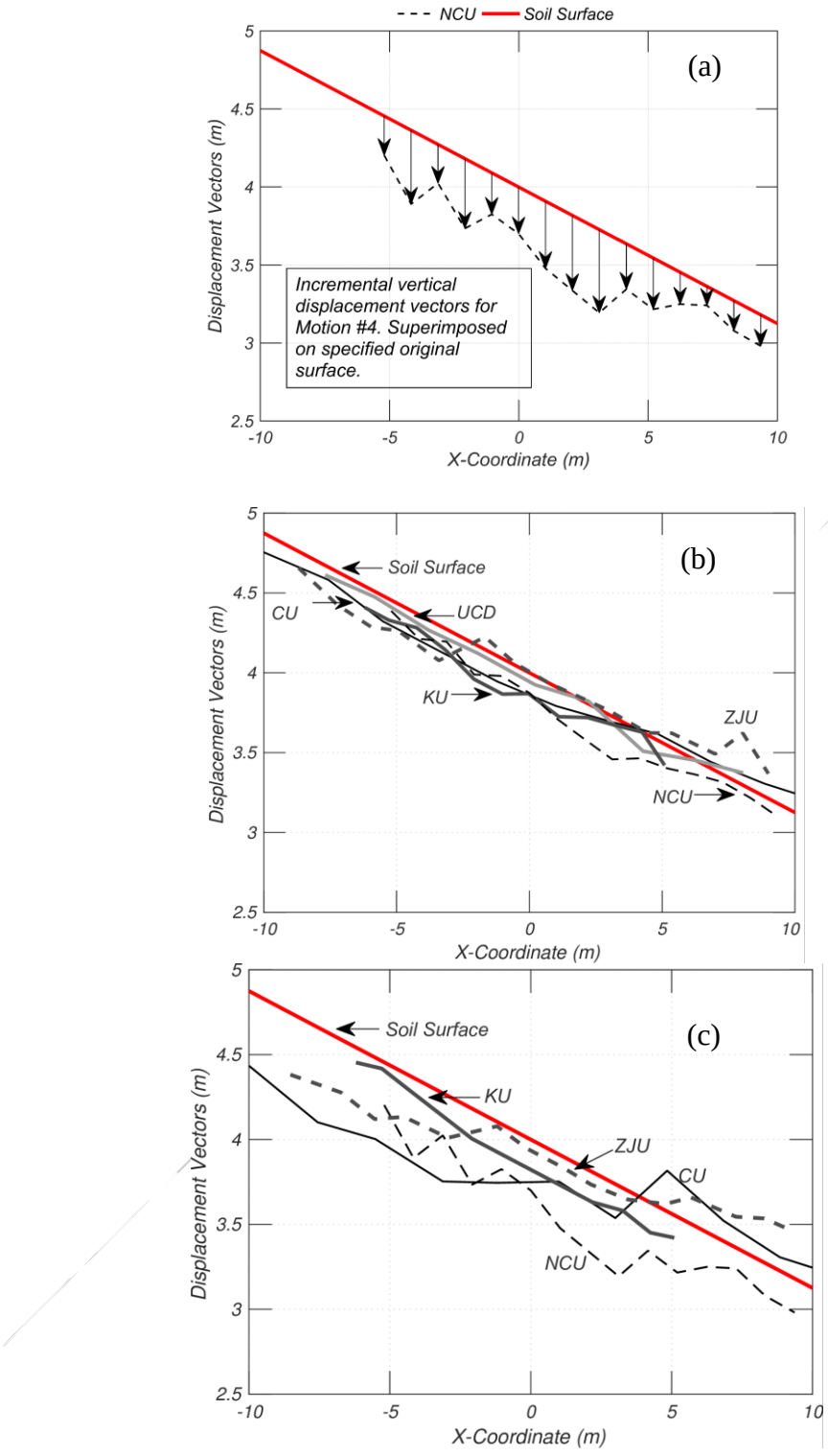

Figure 13: Settlements from surface markers along the longitudinal centerline. (a) example from NCU (Motion #4) showing incremental vertical displacement vectors superimposed on the initial specified slope to illustrate interpretation for figures (b) and (c); (b) incremental settlement for Motion #2; (c) incremental settlements for Motion #4.

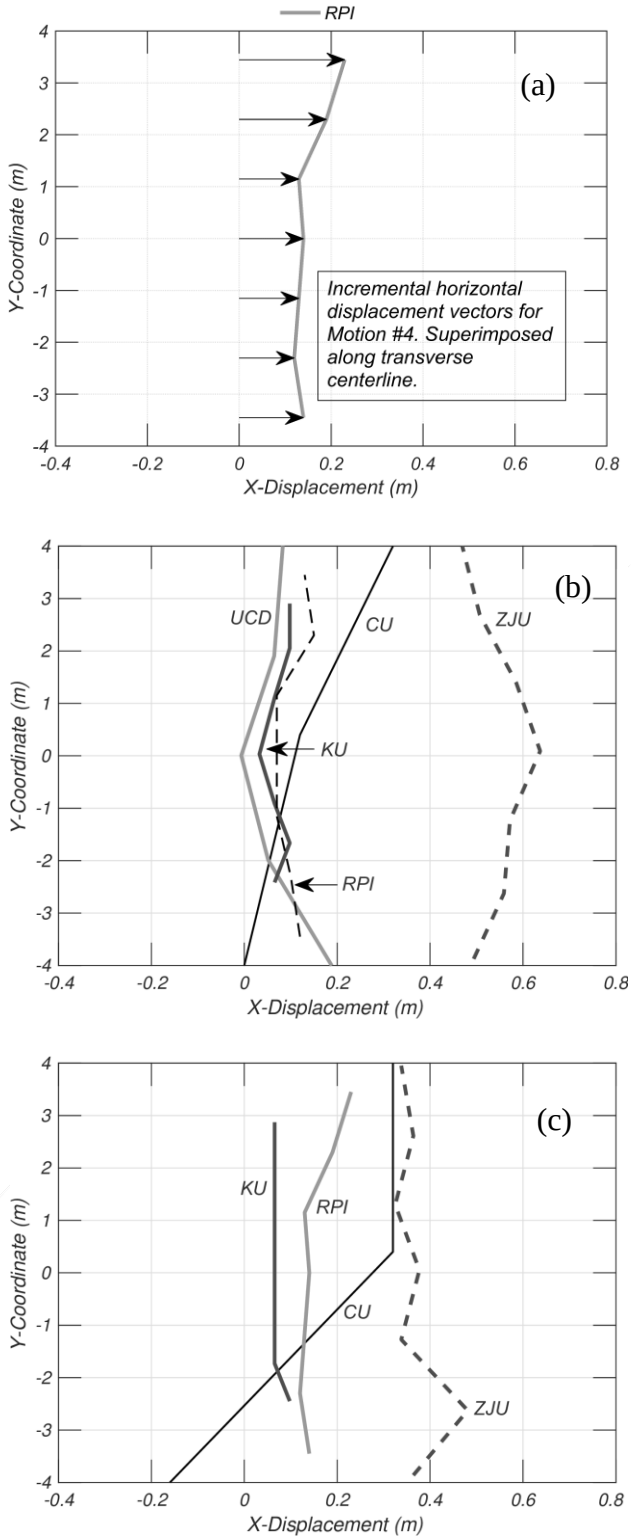

Figure 14: Horizontal displacement from surface markers along transverse centerline. (a) example from RPI (Motion #4) showing displacement vectors to illustrate interpretation for figures (b) and (c). (b) incremental horizontal displacements for Motion #2. (c) incremental horizontal displacements for Motion #4.

The magnitude of the permanent displacement (shown as a gray ramp function) is the average of the lateral displacements in the range of -2 m ≤ y ≤ 2 m in Figures 14. The 4 m range was selected to encompass the central array and AH4. The shape of the permanent displacement ramp follows the "cumulative positive relative velocity (CPRV) of AH4 relative to the base. The CPRV is defined as

$$CPRV = \int_0^\infty \chi[v_{rel}(t)]dt \quad where \ \chi = \begin{cases} 0 & if \quad v_{rel}(t) < 0 \\ 1 & if \quad v_{rel}(t) > 0 \end{cases} \qquad \text{(eq. 4)}$$

where v_{rel} is the relative velocity. Negative velocities were not included in the shape of the relative displacement ramp because it is assumed they will not produce permanent displacements in the downslope direction, consistent with Newmark's sliding block theory (Newmark [24]).

4.6.2 Observation of results

For Motion #2 the base shaking begins at t = 2 s (see Figure 6) but relative displacement is very small until time = 10 s (the time of the peak of the base motion). In other words, before t=10 s, AH4 and the base of the container are moving nearly in unison. CU, UCD and RPI have similar dynamic displacements both in terms of amplitude and duration. KU and NCU have a slightly reduced amplitude and duration.

The relative displacement for Motion #4 begins earlier in the base motion. Hence, the dynamic component has a longer duration than Motion #2, suggesting more shear strain accumulation. The dynamic displacement component has a similar duration for all models, with slight variations in the amplitude.

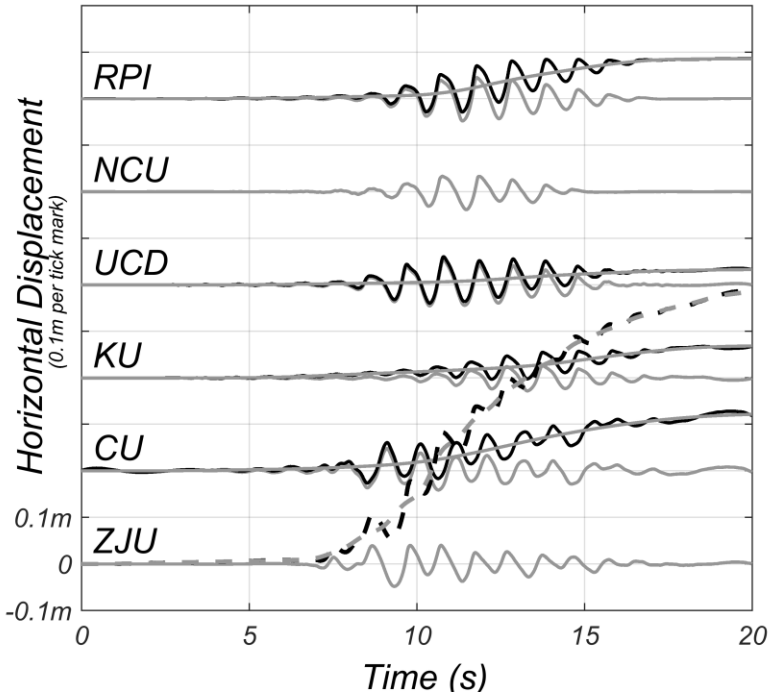

(a) Motion #2

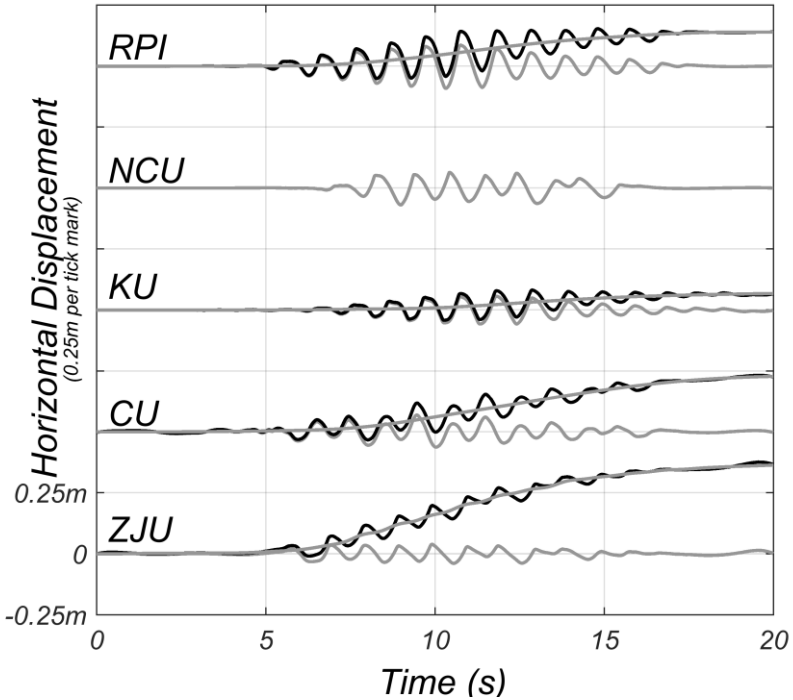

(b) Motion #4

Figure 15: Horizontal displacement for Motions #2 and #4

4.7 Shear Stress-Strain of the Central Array

Figure 16 shows the computed shear stress strain response of the accelerometers of the central array. The stress is calculated at the midpoint between each of the accelerometers (e.g. between AH4 and AH3, AH3 and AH2, etc.). The strain is the average cyclic strain between the accelerometers.

4.7.1 Shear Stress-Strain Curve Generation

The dynamic displacement of the accelerometers is obtained by double integration and baseline correction as described above. The average dynamic shear strain between adjacent accelerometers is obtained the difference between horizontal displacements divided by the spacing of the accelerometers.

The calculation of shear stress at the midpoint of element i, as detailed by Kamai and Boulanger [25] is obtained from Equation 6.

$$\tau_{e,i} = \tau_{e,i-1} + \rho \cdot \frac{z_{i-1} - z_{i-2}}{2} \cdot \left(\frac{3 \cdot a_{i-1} + a_{i-2}}{4}\right) + \rho \cdot \frac{z_i - z_{i-1}}{2} \cdot \left(\frac{3 \cdot a_{i-1} + a_i}{4}\right) \quad \text{Eq. 6}$$

Where ρ is the soil density, and $\tau_{e,i-1}$ is the stress calculated at midpoint of the adjacent element above.

4.7.2 Observations of Results

The stress-strain loops in Figure 16 show overall similar behavior, but there are significant differences in detail. All of the experiments showed evidence of large strains building up and spikes in shear stress associated with the negative pore pressures associated with dilatancy. The results obtained at RPI and KU are quite similar to each other in the sense that the amplitude of shear strains are small at the bottom element of the soil layer (the element below AH1). The other experiments showed larger cyclic shear strains and nonlinear behavior in the bottom element. These observations are all consistent with earlier suggestions that the sand may have been looser at CU and ZJU than at other facilities.

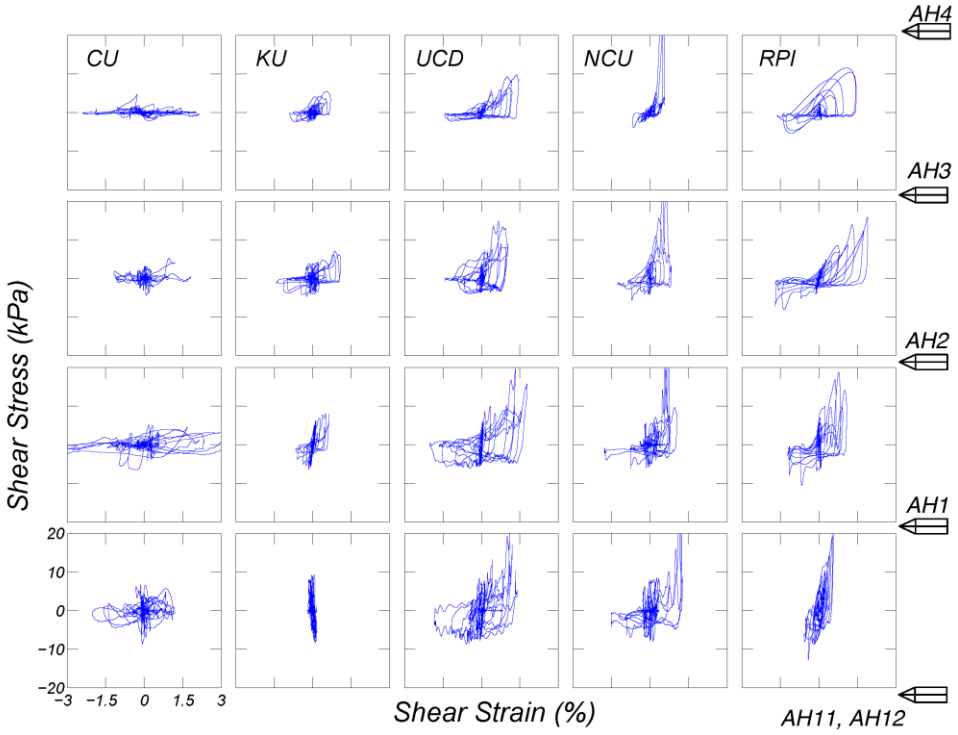

(a)

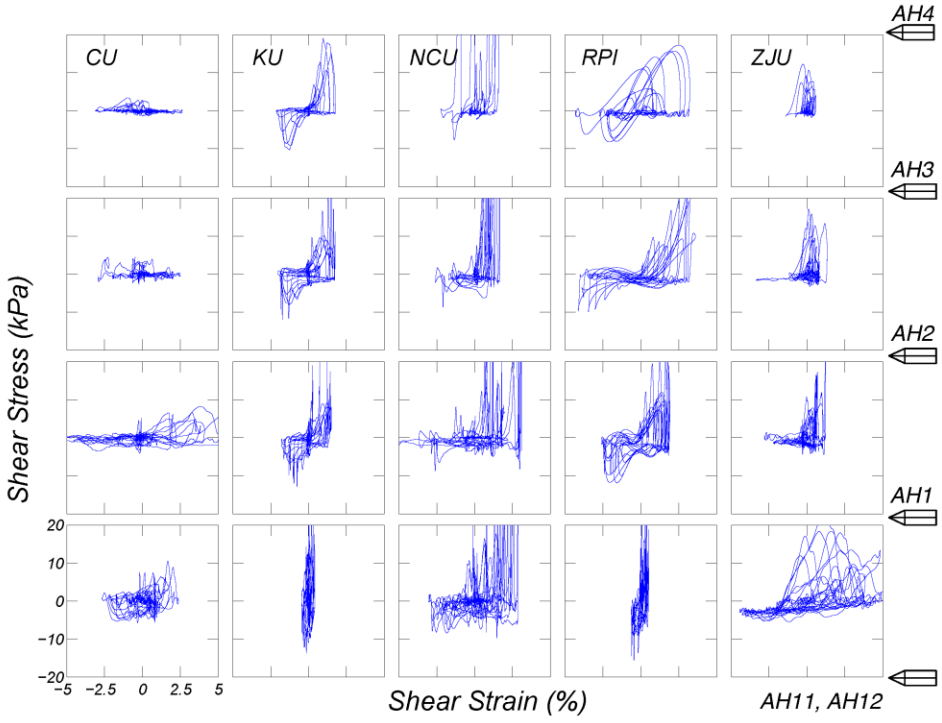

(b)

Figure 16: Shear stress-strain response of the central array for (a) Motion #2 and (b) Motion #4.

5. Conclusions

LEAP-GWU-2015 is one of the first validation efforts within an ongoing LEAP (Liquefaction Experiments and Analysis Projects) program. A centrifuge experiment involving saturated sloping ground was shaken in a rigid box at 6 centrifuge facilities around the world. The specified experiment was a uniform 4 m deep deposit of medium dense sand with a 5 degree slope in a rigid container subject to a ramped, 1 Hz sine wave base motion. The experiment was meant to be relatively simple to enable different facilities to produce comparable experiments. Nevertheless, variations in initial conditions and ground motions led to some differences in results.

The results were shared and archived for the purposes of validation of numerical models during the project and into the future. This paper describes the specification of the experiment and shows general consistency between experimental results. Due to the variety of size, complexity, and uniqueness of the servo-hydraulic shake tables mounted on the various centrifuges, it is not possible to precisely duplicate an experiment at different sites. In addition, the variability and uncertainty in the density of the soil could explain most of the differences. Although they are not identical, when viewed as a whole, the experimental results lend credence to each other. The variability between experiments also provides users of the data a sense of the uncertainty associated with liquefaction experiments on geotechnical centrifuges. Considered together as a group of six experiments, the dataset may be considered to be much more valuable than a single experiment, or even more valuable than one experiment that is repeated six times at a single facility.

Although differences between results of experiments performed at different facilities are larger than ideal, the variability must be understood in the context of the uncertainty of the input parameters (e.g., density, fabric, saturation, sensor locations, distortions due to curvature of the g-field, and ground motions) together may lead to significant differences. It is worth reflecting on considerable variability that is also observed in simple soil mechanics laboratory experiments; for example, the standard deviation of minimum index density was 46 kg/m^3 and 25 kg/m^3 for maximum index density of the Ottawa Sand used in this test program. For the target dry density (1652 kg/m^3), the corresponding $Dr \pm 1\sigma = 65\% \pm 11\%$. An important goal in future validation efforts will be to better interpret comparisons of duplicate experiments in the context of the uncertainty of input parameters and the sensitivity of results to the important uncertainties.

LEAP-GWU-2015 has demonstrated the feasibility of an approach for a next-generation validation database. However, the 2015 exercise is a preliminary step in the validation process. We have now formalized a mechanism and protocol for specification and reporting of round-robin centrifuge experiments that will serve as a strong basis for future efforts. Based upon the data presented and experience gained, there are several suggestions for improvement.

1) Many researchers at many facilities made a great effort to take advantage of this opportunity; the project was completed within a few months of its conception. However, due to time restrictions imposed, the specifications were not followed as rigorously as they could have been. In future LEAP exercises, more time should be allowed to perform the tests, and time should be allocated for repeat of experiments if

errors are made. Human error can be reduced by more careful oversight. Improved communications and researcher exchanges between laboratories would help ensure more precise performance of the experiments according to the intended specification.

2) More rigorous site investigation should be used to confirm the density and saturation of the soils. In-flight shear wave velocity measurement and in-flight CPT testing should be improved and standardized. Zhejiang University did conduct in-flight shear wave velocity measurements Zhou et al. [9]. Shear wave velocity measurements at each facility would be extremely valuable.
3) Improved methods of measuring dynamic displacements of the ground surface of a liquefied deposits would be extremely valuable. Integration of relative acceleration time series data is a reliable method to obtain dynamic displacements at a point, but permanent displacements require another approach. Accurate measurements of before-and-after surface and embedded markers is an important part of the problem. The potential use of high speed, high resolution cameras to measure surface displacements of an array of surface markers may help solve this problem.

Acknowledgements:

The authors of this paper would like to thank the following individuals for their contributions. Eduardo Cerna and Mike Gomez from University of California Davis for providing the SEM imagines of Ottawa F-65 sand. Bao Li (Barry) Zheng assisted with the data processing and plotting of experimental results.

The planning phase of the LEAP project was funded by the US National Science Foundation NEES research program directed by Dr. Richard Fragaszy, through the grants CMMI-1344705, CMMI-1344630, and CMMI-1344619 to the George Washington University, the University of California Davis, and Rensselaer Polytechnic Institute, respectively. The tests of LEAP project performed by National Central University was funded by the Ministry of Science and Technology, R.O.C., research programs directed by Prof. Chung-Jung Lee (MOST 104-2625-M-008-011) and Assistant Professor Wen-Yi Hung (MOST 104-2625-M-008-012), respectively. Part of the work is supported by National Science Foundation of China (No. 51127005) and the National Basic Research Program of China (No. 2014CB047005). Researchers in Japan were partially supported by JSPS KAKENHI Grant Number JP26282103 and JP25420502.

References:

[1] Manzari MT, Kutter BL, Zeghal M, Ghoraiby MEL. Liquefaction Experiments and Analysis Projects (LEAP): Lessons learned. Soil Dynamics and Earthquake Engr (this

issue).

[2] Arulanandan K, Scott RF, editors. Verification of numerical procedures for the analysis of soil liquefaction problems. A.A. Balkema; 1993.

[3] Manzari MT, Kutter BL, Zeghal M, Iai S, Tobita T, Madabhushi SPG, Haigh SK, Mejia L, Gutierrez DA, Armstrong RJ. LEAP projects: Concept and challenges. Proceedings: Fourth International Conference on Geotechnical Engineering for Disaster Mitigation and Rehabilitation (4th GEDMAR): 2014 Sept 16-18; Kyoto, Japan: Taylor and Francis; 2015.

[4] Tobita T, Manzari MT, Ozutsumi O, Ueda K, Uzuoka R, Iai S. Benchmark centrifuge tests and analyses of liquefaction-induced lateral spreading during earthquake. Proceedings: Fourth International Conference on Geotechnical Engineering for Disaster Mitigation and Rehabilitation (4th GEDMAR): 2014 Sept 16-18; Kyoto, Japan: Taylor and Francis; 2015.

[5] Tobita T, Ashino T, Ren J, Iai S. Kyoto University LEAP-GWU-2015 tests and the importance of curving the ground surface in the centrifuge modelling. Soil Dynamics and Earthquake Engr (this issue).

[6] Carey TJ, Hashimoto T, Cimini D, Kutter BL. LEAP-GWU-2015 Centrifuge Test at UC Davis Soil Dynamics and Earthquake Engineering (this issue).

[7] Kokkali, P, Abdoun, T, Zeghal, M. Physical Modeling of Soil Liquefaction: Overview of LEAP Production Test 1 at 2 Rensselaer Polytechnic Institute Soil Dynamics and Earthquake Engineering (this issue).

[8] Hung W-Y, Lee C-J, and Hu L-M. Study of the Effects of Container Boundary and Slope Dip on Soil Liquefaction by Centrifuge Modeling. Soil Dynamics and Earthquake Engineering (this issue).

[9] Zhou, Y.-G., Sun, Z.-B., and Chen, Y.-M. "Zhejiang University benchmark centrifuge test for LEAP and liquefaction responses of a sloping ground." Soil Dynamics and Earthquake Engineering 2016 (this issue).

[10] Madabhushi SSC, Haigh SK, Madabhushi, SPG. LEAP-GWU-2015: Centrifuge and Numerical Modelling of Slope Liquefaction at the University of Cambridge. Soil Dynamics and Earthquake Engineering (this issue).

[11] Carey TJ, Kutter BL, Manzari MT, Zeghal M. LEAP Centrifuge Test and Numerical Simulation Specifications. DOI: 10.17603/DS2159T; 2015.

[12] Carey TJ, Kutter BL, Manzari MT, Zeghal M, Vasko, A. LEAP Soil Properties and Element Test Data. DOI: 10.17603/DS2WC7W; 2016.

[13] Carey TJ, Kutter BL, Manzari MT, Zeghal M. LEAP GWU 2015 Results: Experiments and Predictions. https://nees.org/resources/13616; 2015.

[14] Cerna Alvarez, E. Effects of Particle Weight, Size, Shape, and Size Distribution on Maximum Void Ratio. MS Thesis. University of California, Davis; 2016.

[15] Parra Bastidas AM, Boulanger RW, Carey TJ, DeJong J. Ottawa F-65 Sand Data from Ana Maria Parra Bastidas. DOI: 10.17603/DS2MW2R; 2016.

[16] Lade PV, Liggio CD, Yamamuro JA. Effects of non-plastic fines on minimum and maximum void ratios of sand. Geotech Test J 1998; 21(4):336–47.

[17] Idriss IM, Boulanger RW. Soil liquefaction during earthquakes, MNO–12. Oakland, CA: Earthquake Engineering Research Institute; 2008.

[18] Zeghal M, Goswami N, Kutter BL, Manzari MT, Abdoun T, Arduino P, Armstrong R, Beaty M, Chen Y, Stuart Haigh S, Hung W-Y, Iai S, Kokkali P, Lee C-J, Alborz Ghofrani A, Madabhushi SPG, Tobita T, Ueda K, Zhou Y-G, Ziotopoulou K. Stress-Strain Response of the LEAP Centrifuge Tests and Numerical Predictions. Soil Dynamics and Earthquake Engr (this issue).

[19] Garnier J, Gaudin C, Springman SM, Culligan PJ, Goodings DJ, Konig D, Kutter BL, Phillips R, Randolph MF, Thorel L. Catalogue of scaling laws and similitude questions in geotechnical centrifuge modelling. Int. J. Phys. Model. Geotech, 2007; 8(3):1–23.

[20] Zeghal M, Elgamal A-W. Site response and vertical seismic arrays. Progress in Structural Engineering and Materials, 2000; 2(1):92–101. Invited article.

[21] Kutter BL, Wilson, DW. De-liquefaction shock waves. In: Proceedings of the seventh US–Japan workshop on earthquake resistant design of lifeline facilities and countermeasures against soil liquefaction, Seattle, 1999. p. 295–310

[22] Bonilla LF, Archuleta RJ, Lavallee D. Hysteretic and dilatant behavior of cohesionless soils and their effects on nonlinear site response: field data observations and modeling. Bull Seismol Soc Am, 2005; 95:2373–95.

[23] Abdel-Ghaffar, AM. & Scott, RF. Shear moduli and damping factors of earth dams, J. of the Geotech. Engrg. Div., ASCE, 1979, 105, No. GT12, 1405-1426.

[24] Newmark N. Effects of Earthquakes on Dams and Embankments. Geotechnique 1965:12(2): 139-160.

[25] Kamai R, Boulanger R. Characterizing localization processes during liquefaction using inverse analyses of instrumentation arrays. In: Hatzor YH, Sulem J, Vardoulakis I, editors. Meso-scale shear physics in earthquake and landslide mechanics. The Netherlands: CRC Press/Balkema; 2010. p. 219–38.